

W. Robert J. Funnell, Shyam M. Khanna, & Willem F. Decraemer

On the degree of rigidity of the manubrium in a finite-element model of the cat eardrum

Published in:

Journal of the Acoustical Society of America, 91 (4), Pt. 1, April 1992,
pp. 2082-2090

Copyright (1992) Acoustical Society of America. This article may be downloaded for personal use only. Any other use requires prior permission of the author and the Acoustical Society of America.

doi:10.1121/1.403694

<http://scitation.aip.org/content/asa/journal/jasa/91/4/10.1121/1.403694>

On the degree of rigidity of the manubrium in a finite-element model of the cat eardrum

W. Robert J. Funnell

Departments of BioMedical Engineering & Otolaryngology, McGill University, 3775, rue University, Montréal, Québec H3A 2B4, Canada

Shyam M. Khanna

Department of Otolaryngology, Columbia University, New York, New York 10032

Willem F. Decraemer

Laboratorium voor Experimentele Natuurkunde, Rijksuniversitair Centrum Antwerpen, Antwerpen B-2020, Belgium

(Received 6 November 1990; revised 22 November 1991; accepted 2 December 1991)

It has always been assumed that the manubrium is in effect perfectly rigid. In this paper, a more realistic model of the manubrium is incorporated into an existing finite-element model of the cat eardrum. The manubrial thickness is based on a three-dimensional reconstruction from serial histological sections. After a review of the literature, a value of 2×10^{11} dyn cm⁻² is adopted for the Young's modulus of the bone. The mode of vibration of the model is investigated for different manubrial-thickness values and it is found that a significant degree of manubrial bending occurs in the model for realistic values of manubrial thickness. As a result of the bending, the frequency response at the umbo at high frequencies displays much higher amplitudes and larger phase lags than when the manubrium is rigid. The bending will also affect the displacements transmitted to the ossicular load, and introduce significant errors into estimates of such displacements based on measurements of umbo displacement even at frequencies as low as a few kHz. Recent measurements of manubrium vibrations in the cat ear provide experimental evidence of bending.

PACS numbers: 43.64.Ha, 43.64.Bt, 43.80.Lb

INTRODUCTION

In previous modeling of middle-ear function, it has always been assumed that the manubrium is in effect perfectly rigid. It has also often been assumed that the manubrium has a fixed axis of rotation. Both of these assumptions have been made in our previous finite-element models (Funnell and Laszlo, 1978; Funnell, 1983; Funnell *et al.*, 1987). In the only other three-dimensional quantitative model of the eardrum, Rabbitt and Holmes (1986) also assumed that the manubrium was rigid in their analysis using asymptotic approximations, although they permitted one extra degree of freedom to the ossicular suspension.

Recent experimental data suggest, however, that the manubrium does not always behave perfectly rigidly. We have been using heterodyne laser interferometry to make very precise measurements of the motion of the manubrium in the cat (Decraemer *et al.*, 1990). From experiments in which we measured the vibration at four points on the manubrium (Decraemer *et al.*, 1991), it is quite clear that the manubrium does not move as a rigid body rotating about a fixed axis. There is a strong indication that manubrial bending occurs at high frequencies.

The purpose of this paper is to investigate whether manubrial bending is to be expected on theoretical grounds. In particular, we have included a more realistic representation of the manubrium in our existing finite-element model of the cat eardrum. This paper discusses the actual geometry and

material stiffness of the cat manubrium, introduces these factors into the model, and explores their effects on the motion of the manubrium.

I. GEOMETRY OF THE MANUBRIUM

Important factors in determining the effective stiffness of the manubrium are its cross-sectional shape and size, which vary from the lateral process down to the umbo. The three-dimensional shape of the malleus was measured using a set of serial histological sections from a single cat. The ear was decalcified and embedded in plastic, and sections were cut at 50- μ m intervals. Every second section was stained with hematoxylin and eosin, and mounted.

Since the plane of sectioning was neither parallel to the long axis of the manubrium nor perpendicular to a plane which might be taken as representing the lateral face of the manubrium, measurements could not be taken directly from the serial sections. The malleus geometry was therefore reconstructed in three dimensions on the computer and measurements were taken from the reconstruction. The reconstruction was made by tracing the outlines from a large number of histological sections, and then using the computer to stack them, align them, and generate three-dimensional surfaces joining them. Our reconstruction includes the entire middle ear, and has also been used to model the ossicles as a whole (Funnell and Phelan, 1981) and the posterior incudal ligament (Funnell and Funnell, 1989).

The three-dimensional reconstruction can be rotated to any desired orientation. Figure 1 shows a view of the manubrium with its long axis approximately horizontal and its lateral face approximately perpendicular to the page. The model was graphically sectioned with cutting planes perpendicular to the long axis, at the positions indicated by the cutting-plane lines labeled a to g in Fig. 1. Figure 2 shows the resulting sectional views. The white areas are the cross-sectional surfaces; the shaded areas represent the remainder of the reconstructed manubrium, looking toward the lateral process.

In our previous models, we used a finite-element mesh which is fine enough to represent the longitudinal thickness variations of the manubrium, but which is only one element wide across the manubrium. Since each element has a uniform thickness, this means that the transverse thickness variations of the manubrium cannot be reproduced with this mesh. A mesh several times finer would be required to represent the transverse thickness variations. Since the computational time and storage requirements increase exponentially with increases of the mesh resolution, the additional computational effort would be excessive for our present purposes. We have chosen, therefore, to use the same mesh as in our previous models. This necessitates the calculation of an equivalent thickness to account for the transverse variations.

The three cross sections nearest the lateral process (e–g in Figs. 1 and 2) are all about 0.6 mm wide. The widths of the lower four cross sections (a–d) are 0.7, 1.0, 0.8, and 0.7 mm, respectively. Cross section b is wider than the others but, since it has a very thin lip on the posterior side, its effective width is about 0.8 mm, similar to the others. The width of the manubrium in our existing finite-element model varies from about 0.53 mm at the lateral process to about 0.59 mm at the umbo. It is advantageous to keep the same element geometry for the new model to permit direct comparison with the old model. We shall therefore use the same widths in the new model. Since the bending stiffness of a beam is proportional

to its width and to the cube of its thickness, the width estimates are less critical than the thickness estimates.

The maximal thicknesses of the cross sections vary from about 0.12 mm near the umbo (a) to 1.3 mm near the lateral process (g), and the shapes of the cross sections vary considerably. As noted above, we must estimate equivalent thicknesses for our model manubrium, which has a constant thickness transversely and therefore a rectangular cross section. The effective bending stiffness of a beam is inversely proportional to I , the area moment of inertia about the centroidal axis of its cross section; I itself can be expressed as kbd^3 , where b is the width, d is the thickness, and k depends on the shape. For a triangular cross section, k is 1/3 of that for a rectangular cross section (Roark and Young, 1975, p. 64), so the effective thickness is obtained by multiplying by $(1/3)^{1/3} \approx 0.69$. Similarly, the correction factors are $(1/4)^{1/3} \approx 0.63$ for a diamond-shaped cross section, and $(22/36)^{1/3} \approx 0.85$ for a trapezoidal cross section with the width at the bottom equal to 1/3 of the width at the top. Approximating the first manubrial cross section (a) as diamond shaped thus gives an effective thickness of 0.07 mm. The second and third cross sections (b and c) can be considered to be intermediate between triangular and trapezoidal, so an appropriate multiplying factor is 0.8. The remaining cross sections can reasonably be considered to be rectangular. The effective cross-sectional thicknesses estimated in this way are indicated by open circles in Fig. 3.

Element thicknesses can be specified in our automatic mesh-generation program in terms of two-dimensional quadratic interpolation functions (Bathe, 1982, pp. 196–201) with the thickness assigned to each element being calculated based on the position of its centroid. Interpolation coefficients were chosen to approximately match the estimated

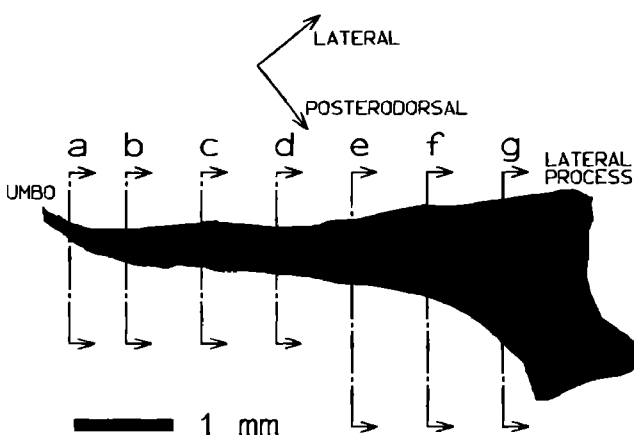


FIG. 1. View of the three-dimensional reconstruction of the manubrium, rotated so that the long axis is horizontal and in the plane of the page. The black curves superimposed on the surface of the reconstruction correspond to the original manubrial outlines traced from the serial histological sections. The cutting-plane lines labeled a to g correspond to the sectional views shown in Fig. 2.

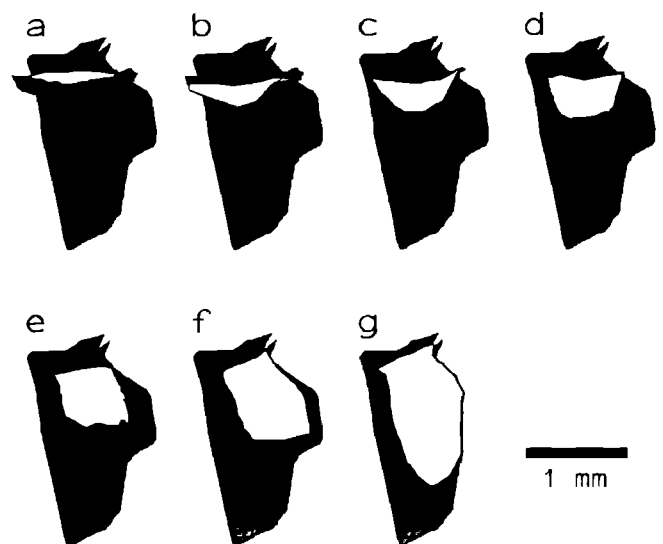


FIG. 2. Sectional views of the three-dimensional reconstruction. The cutting planes are perpendicular to the long axis of the manubrium, at the positions indicated by the correspondingly labeled cutting-plane lines in Fig. 1. The white areas are the cross-sectional surfaces; the shaded areas represent the remainder of the reconstructed manubrium, looking toward the lateral process.

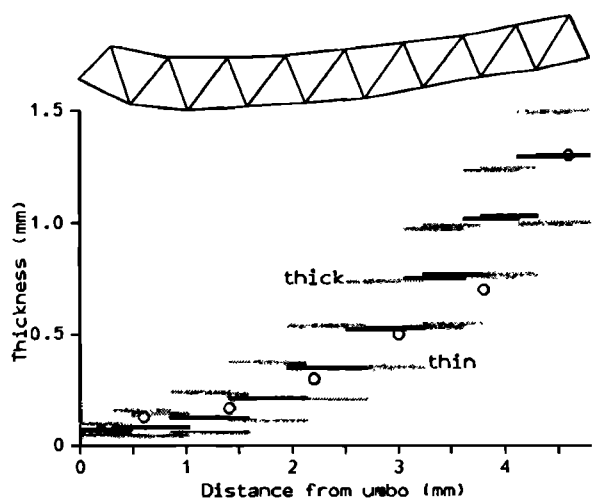


FIG. 3. Effective thicknesses measured from the reconstruction, and the thicknesses used in the finite-element model. The open circles represent the values of effective thickness derived from Fig. 2, as described in the text. The horizontal lines give the thickness values used for the triangular elements of the finite-element mesh for the manubrium shown at the top of the figure. The horizontal extent of each line corresponds to the horizontal extent of one of the triangles, over which the thickness remains constant. The black lines give the thickness values for the *medium*-thickness case referred to in the text. The horizontal gray lines represent two additional sets of thickness parameters, referred to as *thick* and *thin* in the text.

effective thicknesses, and the horizontal black lines in Fig. 3 represent the resulting interpolated thicknesses. The gray horizontal lines in Fig. 3 indicate two additional sets of element-thickness parameters that are used below to explore the effects of varying the overall thickness of the manubrium. On the lower half of the manubrium (0–2.5 mm from the umbo), the element thicknesses for the *thin* set of parameters are approximately 0.5–0.7 times the thicknesses for the *medium* set. Since the bending stiffness is proportional to the cube of the thickness as discussed above, the effective stiffnesses for the *thin* set of parameters are approximately 0.1–0.4 times the stiffnesses for the *medium* set. For the *thick* set of parameters in Fig. 3, the thicknesses on the lower half of

the manubrium are approximately 1.4–1.9 times those for the *medium* set, and the effective stiffnesses are thus approximately 3–7 times those for the *medium* set.

II. MATERIAL STIFFNESS OF BONE

The material stiffness of bone varies widely with the species, the nature of the bone (e.g., cancellous or dense), the direction of measurement (longitudinal or crosswise), and the part of the bone (e.g., end or middle, cortex or interior). In order to obtain an upper limit for our estimate of its stiffness, we shall consider the properties of dense cortical bone. Most measurements have been made in long bones, usually the femur. We shall consider here only longitudinal measurements, as the transverse values are lower. The values of Young's modulus for bone determined by various authors are summarized in Table I. The values range from 0.4×10^{11} dyn cm⁻² for fetal cranium to 3.13×10^{11} for whale tympanic bulla, but for long bones the values are between 1.35×10^{11} and 2.74×10^{11} dyn cm⁻². The highest values are for dry specimens as opposed to fresh ones.

It is not at all clear how the micromechanical structure of the manubrium compares with the structures of the bone tissues for which data are available. We shall take a value of 2×10^{11} dyn cm⁻² as a plausible estimate for Young's modulus of the manubrium.

In estimating the stiffness of the manubrium, we have assumed that it consists of uniform compact bone. In fact, however, the malleus consists of an outer layer of compact bone with less dense bone inside (Kirikae, 1960, pp. 64–65). This may mean that the effective stiffness is less than that estimated here.

III. FINITE-ELEMENT MODEL

Except for the inclusion of a nonrigid manubrium, the finite-element model of the cat eardrum presented here is identical to our previous models (Funnell, 1983; Funnell *et al.*, 1987). The calculated displacements are therefore

TABLE I. Young's modulus of bone as measured by a number of investigators. The data of Lang (1969), Reilly and Burstein (1975), and Yoon and Katz (1976) are from a review by Hayes (1978). The data of Cowin *et al.* (1987) are from a theoretical study by Rice *et al.* (1988).

Source	Species	Type	State	Young's modulus $\times 10^{11}$ dyn cm ⁻²
Lang (1969)	bovine	femur	dry	2.60
Reilly and Burstein (1975)	bovine	femur	fresh	2.26
Reilly and Burstein (1975)	human	femur	fresh	1.70
Yoon and Katz (1976)	human	femur	dry	2.74
Gibbons (1976)	human	"typical"	"typical"	1.74
Currey (1979)	bovine	femur	dry	1.35
Cowin <i>et al.</i> (1987)	bovine	?	?	1.8–2.2
Cowin <i>et al.</i> (1987)	human	?	?	1.7–2.0
Currey (1979)	whale	tympanic bulla	dry	3.13
McPherson and Kriewall (1980)	human	fetal cranium	fresh	0.4

directly comparable to the results in the previous papers. The triangular finite-element mesh is generated with a nominal resolution of 12 elements/diameter (Funnell, 1983). The pars tensa has a thickness of $40\text{ }\mu\text{m}$, a density of 1.0 g cm^{-3} , a Young's modulus of $2 \times 10^8\text{ dyn cm}^{-2}$, and a Poisson's ratio of 0.3; its overall three-dimensional shape is defined by a normalized radius of curvature equal to 1.19. The damping parameters α and β are 1500 s^{-1} and 0 s, respectively. The acoustical stimulus is a uniform pressure of 100 dB SPL. There is no acoustical load due to the middle-ear air cavities, that is, the middle-ear septum and bulla are considered to be opened widely.

The present model has a fixed axis of rotation as in our previous models. This assumption appears to be valid for low frequencies, and it permits us to focus on the effects of manubrial bending alone. The combined ossicular and cochlear load is represented by a single lumped rotational impedance at the fixed axis, consisting of (1) a stiffness of $14 \times 10^3\text{ dyn cm}$, (2) damping specified by the same damping parameters α and β as the eardrum, and (3) a moment of inertia of 0.2 mg cm^2 . As in the previous models, this moment of inertia includes the mass of the manubrium, and the manubrial elements themselves have zero mass. This permits us to investigate the effects of varying the manubrial thickness without being disturbed by concomitant changes in manubrial mass.

Frequency responses are obtained by computing a step response using direct integration in the time domain, differentiating to obtain the impulse response, and then doing a fast Fourier transform. All model displacements presented here are the nodal-displacement components perpendicular to the plane of the tympanic ring—the tympanic ring is in the x - y plane as shown in Fig. 4, and the z components of displacement are calculated.

It has been shown earlier that the behavior of this model compares quite well with experimental results (Funnell *et al.*, 1987; Decraemer *et al.*, 1989). The low-frequency umbo displacement in the model is approximately 250 nm. Reducing this value by 5 dB to allow for the effect of a closed bulla (Guinan and Peake, 1967) gives about 140 nm, which is only about 3 dB lower than the typical value of 200 nm given by Khanna and Tonndorf (1972) and well within the range of individual variability.

In our previous models, the perfect rigidity of the manubrium was obtained with a master/slave mechanism (Funnell and Laszlo, 1978). The manubrium was assumed to rotate about a fixed axis parallel to the x axis. A single rotational degree of freedom was assigned to this axis, and the degrees of freedom of nodes on the manubrium were forced to correspond exactly to a rotation about the axis. This meant that elements needed to be defined explicitly only for the part of the malleus actually embedded in the eardrum and not for the neck and head. In the present model, the behavior of the malleus is modeled with actual elements having finite stiffness, rather than with the master/slave mechanism. This means that new elements must be added to model the neck of the malleus, and the heads of the malleus and incus. The shapes of these elements are not important since they are assumed to be thick enough to be effectively rigid, and they are again massless; they serve only to attach the

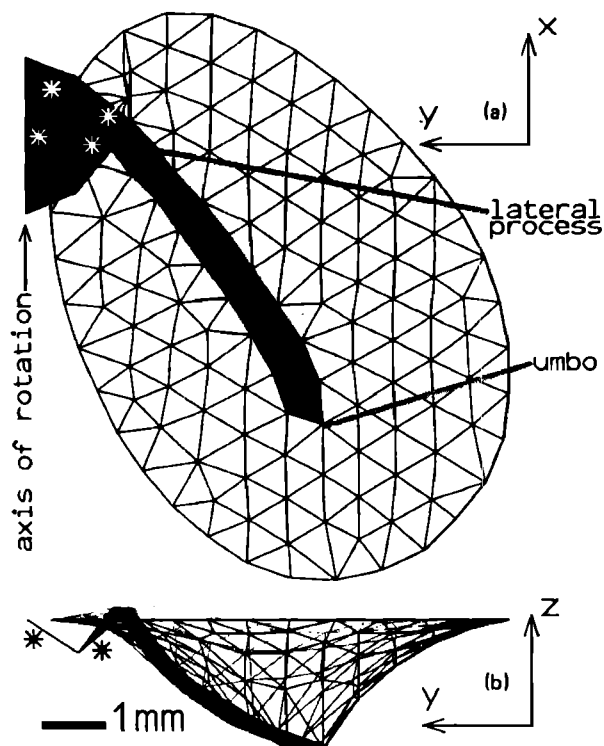


FIG. 4. Finite-element model of the eardrum, manubrium, and malleolar neck. (a) Model viewed along the z axis. (b) View along the x axis. The triangular elements corresponding to the malleus are filled in, while those corresponding to the eardrum are plotted as a wire frame. The asterisks indicate the four elements corresponding to the head and neck of the malleus.

manubrium to the axis of rotation. They have been modeled as a set of four triangular plates with a thickness of 1.5 mm. Figure 4 shows how they dip behind the eardrum and join the lateral process of the malleus to the assumed axis of rotation. Since they are behind the eardrum, no sound-pressure load is applied to them, although it is applied to the elements of the manubrium proper.

IV. RESULTS

Before investigating the effects of the finite stiffness of the manubrium, we must first establish that the new model is capable of giving the same results as the old model that had a perfectly rigid manubrium. Figure 5 presents frequency responses of a point on the lateral process of the manubrium. The thick gray curves were computed with the old model; the thin black curves were computed with the new model using a constant manubrial thickness of 1.5 mm, which is thick enough that the manubrium does not bend significantly. It can be seen that the curves from the two models are almost identical, indicating that the old master/slave manubrium model and the new explicit manubrium model are essentially equivalent. Figure 5 also presents a frequency response calculated for a model with a finite-element mesh generated at 15 elements/diameter rather than 12. This frequency response is almost identical to the others up to 6 kHz, and the amplitude differences are only a few dB all the way to 15 kHz. This indicates that the lower-resolution mesh is ade-

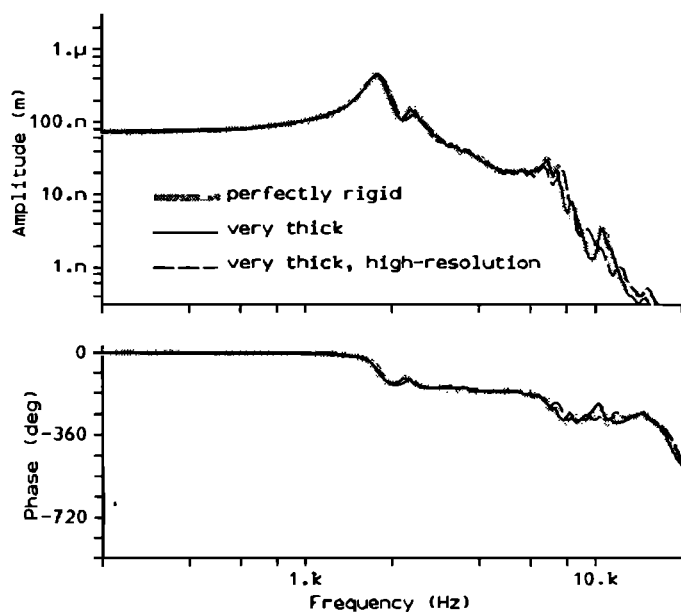


FIG. 5. Comparison of the frequency response of the model having a perfectly rigid manubrium (Funnell *et al.*, 1987) with that of the new model with a very thick manubrium. The displacements in all figures are calculated for a pressure of 100 dB SPL at the eardrum. The thick gray lines correspond to the old model. The thin black solid lines show the response of the new model with a manubrium of constant thickness = 1.5 mm. The dashed lines show the response of a model with a higher-resolution finite-element mesh (15 elements/diameter rather than 12). This model also has a constant manubrial thickness of 1.5 mm.

quate at least for studying manubrial behavior within this frequency range.

Figures 6 and 7 present displacements calculated for nodes along the length of the malleus, for the three sets of manubrial-thickness values specified in Fig. 3. Figure 6 includes frequencies from 0–4 kHz and Fig. 7 includes frequencies from 5 kHz up to 10 kHz. Within each cell of the two figures, the horizontal axis gives the projected perpendicular distance from the axis of rotation, measured along a line parallel to the *y* axis (see Fig. 4). On the vertical axis are plotted the nodal displacements at the instant of time at which the lateral process reaches its maximal displacement. Note that the displacement scale is expanded in Fig. 7. The gray parts of the curves correspond to the head and neck of the malleus; the black parts correspond to the manubrium, from the lateral process on the left to the lower tip (at the umbo) on the right. The malleus has zero displacement at the axis of rotation; the head and neck remain rigid in every case. The upper part of the manubrium itself also remains rigid, but its lower part bends more and more as the frequency increases and as the thickness decreases. In the top row of cells in the two figures, where the manubrium is thickest and thus most stiff, it remains essentially rigid up to 5 kHz. At 6 and 7 kHz, the triangles of the finite-element mesh are visible, which means that points at the same distance from the axis but on opposite sides of the manubrium have different displacements; this implies that the manubrium is twisting as well as bending. In the middle row, with intermediate thickness, the bending is significant by 3 kHz, and by 7 kHz the bending and twisting are quite dramatic. In the lower row of cells, with a manubrium which is even thinner and

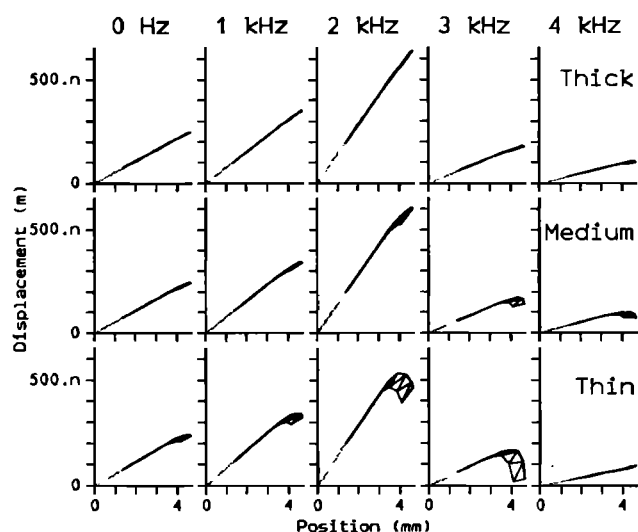


FIG. 6. Manubrial displacement as a function of position along its length, for frequencies from 0 to 4 kHz, for three different sets of manubrial-thickness parameters—*thick* in the top row, *medium* in the middle row, and *thin* in the bottom row. Within each cell, the horizontal axis represents the perpendicular distance (measured along a line parallel to the *y* axis of Fig. 4) from the axis of rotation to the nodes of the finite-element mesh. The vertical axis in each cell is nodal displacement. Within each cell, the displacement for each node is calculated for the particular instant of time at which the lateral process reaches its maximal displacement; i.e., the displacement plotted for node *i* is $d_i = A \cos(\phi_i - \phi_{LP})$, where ϕ_{LP} is the phase at the lateral process. The gray parts of the curves correspond to the head and neck of the malleus, the black parts correspond to the manubrium.

thus less stiff, similar patterns occur at even lower frequencies—the bending is already extreme by 3 kHz.

In interpreting the manubrial displacement profiles of Figs. 6 and 7, it must be kept in mind that there can be large phase variations along the length of the manubrium. This is demonstrated in Fig. 8 for three different cases. The two top rows correspond to 7 and 10 kHz, respectively, for the medium-thickness manubrium. The bottom row corresponds to 5 kHz for the thin manubrium. For each row, the displace-

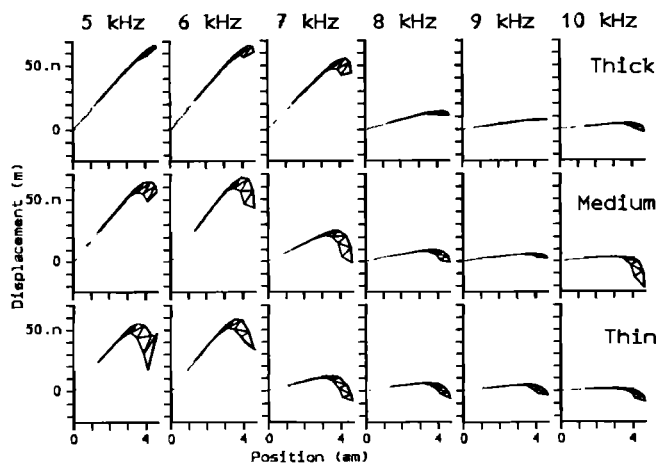


FIG. 7. Manubrial displacement as a function of position along its length, for frequencies from 5 to 10 kHz. The format is the same as for Fig. 6 but the displacement scales are magnified.

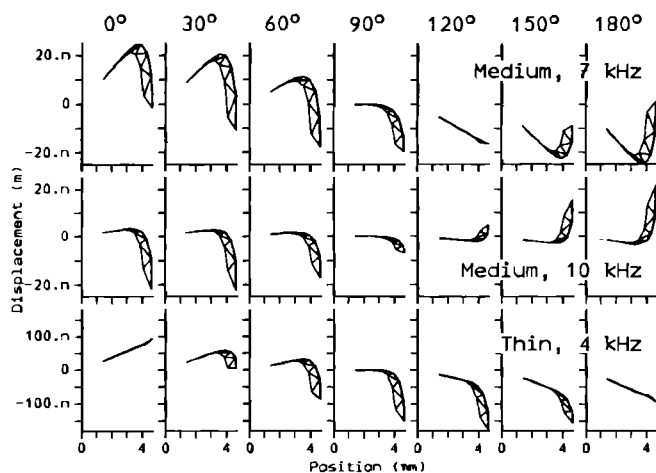


FIG. 8. Manubrial displacement as a function of position along its length, for seven different instants of time during one half-cycle of vibration. Three different cases are shown. The top and middle rows are for the medium-thickness manubrium at 7 and 10 kHz, respectively. The bottom row is for the thin manubrium at 4 kHz. Here, 0° refers to the instant of time at which the lateral process reaches its maximal displacement.

ment profile of the manubrium is shown for seven different instants of time during one half-cycle of vibration. The column marked 0° corresponds to the instant of time shown in Figs. 6 and 7, at which the maximal displacement of the part of the manubrium near the lateral process occurs. For the medium-thickness manubrium at 7 kHz (top row), it is seen that the inferior tip of the manubrium has its maximal negative displacement at about 90° , and zero displacement at about 0° . Thus there is a 90° phase difference between the lateral process and the umbo. In the middle row, on the other hand, at 10 kHz, the manubrial tip has its maximal displacement at 180° . At 4 kHz, for the thin manubrium (bottom row), the manubrial tip has its greatest negative displace-

ment at 120° . As a result the manubrium happens to be almost completely unbent at 0° and 180° .

The effect of manubrial bending on the effective input to the middle ear can be evaluated in terms of the displacements at the lateral process, since there is no significant bending of the head and neck of the malleus in the model. Figure 9 shows frequency responses calculated for the same node on the lateral process that was used for Fig. 5. The thick gray curves represent the case of the very thick, effectively rigid, manubrium, as a reference. It can be seen that at the lowest frequencies there is a very small increase of displacement as the manubrium becomes thinner—the increase is about 2% and 6% for the *medium* and *thin* cases, respectively. The frequency-response amplitudes for the medium-thickness and thin manubria are within 1 dB ($\sim 10\%$) of the rigid-manubrium case up to about 2.2 and 1.1 kHz, respectively, and within 2 dB ($\sim 25\%$) up to about 4.3 and 1.6 kHz. The differences reach +3 dB by 6.3 and 2.2 kHz, respectively. Above these frequencies the amplitude differences are increasingly variable, and are predominantly decreasing. The greatest increases are about 6 dB, while the greatest decreases are 8.6 dB for the medium case and 13.9 dB for the thin case. There are also significant phase changes, practically all in the direction of increased phase lag. For the medium case, the phase changes are largest in the vicinity of 6 kHz, and above 12 kHz. For the thin case, there is another region of large phase change between 3 and 4 kHz.

The effects of the bending become much greater as we go further down the manubrium, at least at high frequencies. Figure 10 presents frequency responses in the same format as Fig. 9, but this time for a node at the umbo. Here the frequency-response amplitudes at very low frequencies for the medium and thin manubria are slightly lower (less than 1%) than those for the rigid manubrium; leading up to the peak at 1.8 kHz, they become somewhat higher (up to 7%) than the rigid-manubrium amplitudes. The amplitudes for the medi-

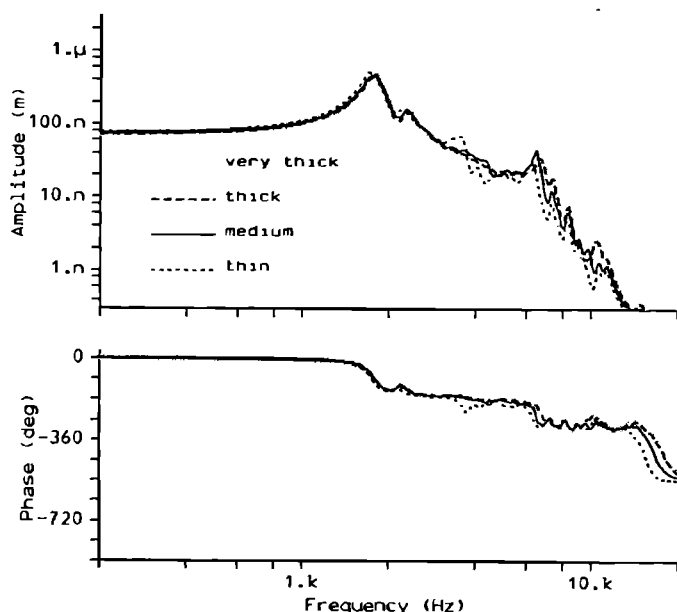


FIG. 9. Model frequency responses for a node on the lateral process. The *very-thick* curves correspond to the 1.5-mm case shown in Fig. 5. The *thick*, *medium* and *thin* curves correspond to the three thickness cases shown in Figs. 6 and 7. Differences in response are small.

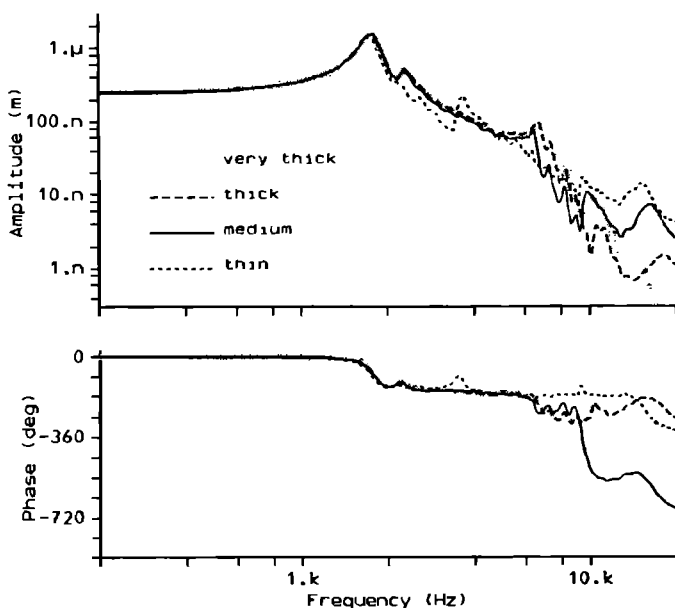


FIG. 10. Model frequency responses for a manubrial node at the umbo. The four thickness cases are the same as in Fig. 9. Differences in response are large, particularly at frequencies above 10 kHz.

um-thickness manubrium remain within 2 dB of the rigid-manubrium case up to about 6.6 kHz; for the thin manubrium, however, the amplitude already differs by 6 dB at 2.5 kHz. Up to 10 kHz, the amplitudes for the medium-thickness and thin manubria are both generally lower than the rigid-manubrium amplitudes, and both remain within 15 dB of the rigid case; the phase differences become quite marked above roughly 6 kHz.

The most striking feature of these curves, however, is in the range from 10–20 kHz, where the amplitude for the flexible manubrium stays relatively high instead of decreasing rapidly as it does for the rigid manubrium. The result is an amplitude difference that at 18.3 kHz reaches 32 and 35 dB for the medium and thin cases, respectively. For the manubrium of medium thickness, there is also a sharp increase of almost 360° in the phase lag above 9 kHz. (Note that the frequency resolution in these curves is 100 Hz, so this sharp change is not due to the 360° ambiguity inherent in phase unwrapping.) The amplitude plateau in the range from 10–20 kHz, and the large values of phase lag, have been observed experimentally (Decraemer *et al.*, 1991).

V. DISCUSSION

The model results obtained here for realistic dimensions and material stiffness indicate that the cat manubrium can be expected to undergo considerable bending and twisting at frequencies above a few kHz, and possibly at frequencies as low as 1 or 2 kHz. The effect on frequency responses measured near the umbo is quite pronounced, especially above 10 kHz, where the displacement amplitude remains relatively high instead of dropping rapidly as it does in the model with a rigid manubrium. This may at least partially explain a difference that has been noted before between experimental observations and model results (Funnell *et al.*, 1987).

Mention has been made earlier of our recent experiments in which evidence of high-frequency manubrial bending was seen (Decraemer *et al.*, 1991). In a further experiment using the same techniques, the vibration was measured at a larger number of points on the manubrium. At each point, measurements were made over a broad range of frequencies. The time intervals between measurements at different points were from 28–65 min; the frequency sweeps at each point took less than 10 min each. The original aim of the experiment was to investigate the three-dimensional motion of the manubrium, and the data will be analyzed and presented more fully elsewhere. In view of the modeling results obtained here, however, we have analyzed some of the low-frequency data to look for evidence of manubrial bending.

Six of the measurement points were distributed from the umbo almost all the way up to the lateral process. Figure 11 presents data from four consecutive frequencies, from 1.34–2.08 kHz. The open circles indicate the positions of the six points on the manubrium, and their displacement amplitudes. (At any one frequency, the phase differences among the six points were all less than 12°.) A straight line has been fitted to the amplitudes for the first frequency and plotted as a gray line. When projected to the left, it intersects the horizontal axis at a point which corresponds to the position of a fixed axis of rotation. The same straight line has also been

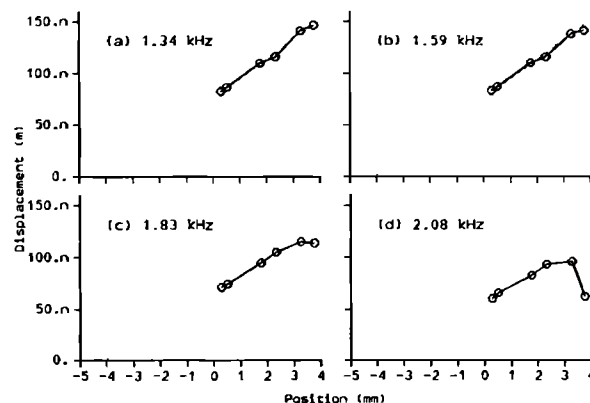


FIG. 11. Displacement data for six points on the cat manubrium for 100 dB SPL at the eardrum, at four consecutive frequencies. The open circles indicate the positions of the six points on the manubrium, measured from the lateral process. For each frequency the displacements are plotted for the value of phase which gives maximal displacements. (a) 1.34 kHz—a straight line (gray) has been fitted to the data, and extrapolated to the apparent axis of rotation. (b) 1.59 kHz—the gray line is the same as in part (a). (c) and (d) 1.83 and 2.08 kHz—the gray line joins the first point on the manubrium to the apparent axis position from part (a). Bending is most pronounced at 2.08 kHz.

plotted for the second frequency and again is seen to fit the data well. Thus, the data at the first two frequencies indicate that (1) the preparation is stable over the time intervals between measurements at different points; (2) the manubrium is vibrating about an axis of rotation which is fixed during the vibration cycle; and (3) the manubrium is vibrating as a rigid body.

At the third and fourth frequencies, and especially the fourth, straight lines do not fit the data in the region of the umbo. In each case, therefore, instead of attempting to fit a straight line to all six points, we have drawn a straight line from the leftmost measurement point to the point representing the axis of rotation from the first frequency. It can be seen that in each case the first four data points are almost colinear with the line drawn from the presumed rotational axis, indicating that the axis has not moved. The data points nearer the umbo, however, fall significantly below an extrapolation of this line. The effect is larger at the fourth frequency. Although further experimental investigation is clearly required, these observations are consistent with the suggestion of low-frequency manubrial bending.

As noted in Sec. II, the value chosen for Young's modulus, $2 \times 10^{11} \text{ dyn cm}^{-2}$, is on the high side of the observed range of values for compact bone. Furthermore, the estimate did not take into account the fact that the manubrium is not uniform throughout, and the presence of less dense bone in the interior could reduce the overall stiffness. Therefore, the flexibility of the manubrium may actually be even greater than in the model presented here.

With our assumption in the current model of a fixed axis of rotation, the rotational displacement at the axis is the ultimate output of the eardrum/manubrium system, and its amplitude is a measure of the effectiveness of the coupling of ear-canal acoustical pressure to middle-ear mechanical displacement. Since the head and neck of the malleus are effec-

tively rigid in our model, the displacements at the lateral process are a direct measure of the rotation about the axis. On this basis, the bending of the manubrium seems to result in a slight increase of efficiency of the system at very low frequencies, an increase of a few dB at frequencies up to a few kHz, and mostly decreases of up to 10–15 dB at higher frequencies.

In principle, in a system like this where a long embedded beam serves to transmit energy from a large flexible shell (or membrane) to a stiff hinge, increased flexibility of the beam can either increase or decrease the resulting rotational displacement at the hinge. Making the beam more flexible can *increase* the coupling by decreasing the constraints that the beam places on the displacement of the shell. Clearly, there is a limit to how flexible the beam should be, however, since in the extreme case, there would be effectively no beam at all and the coupling would be very poor between the flexible shell and the stiff hinge. Thus excessive flexibility of the beam will *decrease* the coupling. Presumably, the reason our results show mixed and relatively small effects of manubrial bending on the effectiveness of the coupling is that the two factors are closely balanced over the range of parameters explored—as the manubrium becomes more flexible, it loses some of the force contribution from its tip, but at the same time, the tip interferes less with the vibration of the eardrum.

The coupling between the eardrum and the manubrium is a case of impedance matching, analogous to the impedance matching required between the air in the ear canal and the liquid in the cochlea. The fact that the manubrium is tapered may be seen as an attempt to avoid an abrupt impedance change, by gradually decreasing the stiffness from the thick and rigid head and neck of the malleus toward the center of the relatively flexible eardrum. (Of course, the tapering also reduces the moment of inertia of the manubrium about the axis of rotation, reducing its contribution to the increasing impedance at high frequencies. Recall that the modeling approach presented here has excluded this mass effect since the mass of the malleus is all contained in a fixed moment-of-inertia term. This also means that none of the bending observed here can be due to resonances of the manubrium itself.)

The motion of the manubrium is determined by the combined effects of (1) the forces exerted on it by the eardrum; (2) the forces exerted on it by the ossicular and cochlear loads; (3) its own inertial and damping forces; and (4) the acoustical forces acting directly on it, which are small. The bending of the manubrium is presumably determined primarily by the interaction between the ossicular load and the eardrum forces. The spatial distribution of the eardrum forces depends on the pattern of eardrum vibration, which changes dramatically with frequency. The bending can thus be expected to be quite different at different frequencies. At very high frequencies, the acoustical pressure distribution over the surface of the eardrum is nonuniform (Khanna and Stinson, 1985; Stinson, 1985). This nonuniformity, which has not yet been included in our model, may contribute to the strong bending that appears experimentally at very high frequencies (Decraemer *et al.*, 1991).

The most important immediate consequence of the

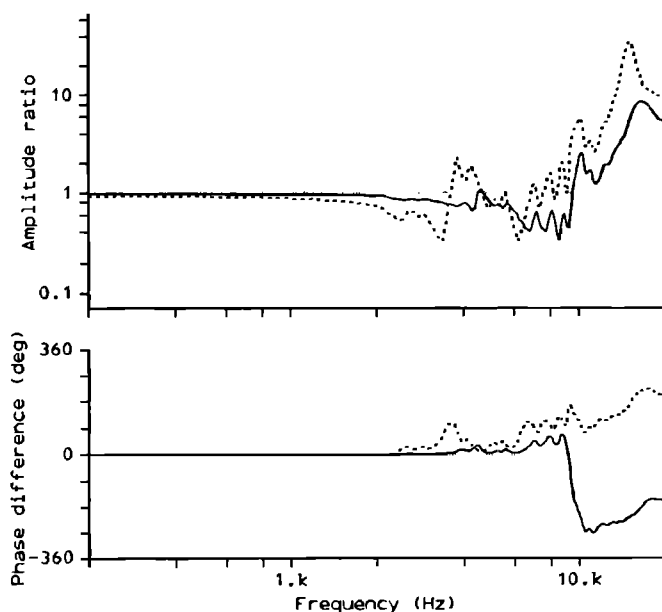


FIG. 12. Amplitude ratio and phase difference comparing displacement of the lateral process with the displacement that would be estimated for it based on the displacement at the umbo, assuming a rigid manubrium and a fixed axis of rotation; i.e., the amplitude and phase of the quotient G_c/G_p , where G_p is the complex-valued displacement of the lateral process, and the estimate is given by $G_c = k G_u$, where G_u is the displacement of the umbo and k is the ratio of the distances from the axis of rotation to the two points. The solid line is for the medium-thickness manubrium, the dashed line is for the thin manubrium. Departures from the horizontal gray lines represent errors in the estimated displacement.

observation that the manubrium may bend lies in the error it would introduce into any experimental attempt to quantify middle-ear input using measurements of manubrial displacement. Figure 12 focuses on this effect by presenting the amplitude and phase errors due to predicting lateral-process displacements based on umbo displacements. The errors are plotted as functions of frequency for the models with medium-thickness and thin manubria. For the medium-thickness manubrium, the error at very low frequencies is about 3%; by 2 kHz, it has increased to 7%, and by 4 kHz, it is 22%. Between 6 and 10 kHz, the error is as high as 66%; above 10 kHz, the error changes sign and again becomes quite large. Also, above 10 kHz, there is a phase error of as much as 272°.

As pointed out above, the medium-thickness manubrium used here may well underestimate the flexibility of the manubrium. With this in mind, we see that the errors in Figure 12 are even larger for the thin-manubrium case. They increase from 7% at very low frequencies, to 11% at 1 kHz, to 67% at 3.4 kHz. Above this frequency the error is strongly frequency dependent and often changes sign abruptly. There are also significant phase errors, already reaching 25° at 2.5 kHz; the phase error above 10 kHz is very different from that for the medium-thickness case. If the manubrium does bend as suggested by these modeling results, it implies that manubrial displacements cannot easily be used to characterize experimental input to the inner ear even at low frequencies.

The effect of the bending in the model varies from being relatively small for the thick manubrium to being quite large

for the thin manubrium. This shows that, within anatomically and physiologically reasonable ranges, the behavior of the system depends strongly on the actual shape and mechanical properties of the manubrium. Since anatomical variations among individuals can be sizable, this in turn implies that there may be considerable differences in manubrial bending among individuals, particularly among different age groups. There are also presumably differences among species. Further experimental work is clearly required to study the extent and significance of manubrial bending.

ACKNOWLEDGMENTS

This work was supported by the Medical Research Council of Canada. The experimental part of this work was carried out at the Fowler Memorial Laboratory of Columbia University, supported by NIDCD Grant No. DC 00316 and by the National Scientific Research Foundation of Belgium. We thank J. Lauzière for editing the manuscript.

- Bathe, K.-J. (1982). *Finite Element Procedures in Engineering Analysis* (Prentice-Hall, Englewood Cliffs, NJ).
- Cowin, S. C., Van Buskirk, W. C., and Ashman, R. B. (1987). "The properties of bone," in *Handbook of Engineering*, edited by A. Skalak and S. Chien (McGraw-Hill, New York), pp. 2-1-2-27.
- Currey, J. D. (1979). "Mechanical properties of bone tissues with greatly differing functions," *J. Biomech.* **12**, 313-319.
- Decraemer, W. F., Khanna, S. M., and Funnell, W. R. J. (1989). "Interferometric measurement of the amplitude and phase of tympanic membrane vibrations in cat," *Hear. Res.* **38**, 1-17.
- Decraemer, W. F., Khanna, S. M., and Funnell, W. R. J. (1990). "Heterodyne interferometer measurements of the frequency response of the manubrium tip in cat," *Hear. Res.* **47**, 205-217.
- Decraemer, W. F., Khanna, S. M., and Funnell, W. R. J. (1991). "Malleus vibration mode changes with frequency," *Hear. Res.* **54**, 305-318.
- Funnell, W. R. J., and Laszlo, C. A. (1978). "Modeling of the cat eardrum as a thin shell using the finite-element method," *J. Acoust. Soc. Am.* **63**, 1461-1467.
- Funnell, W. R. J., and Phelan, K. E. (1981). "Finite-element modeling of the middle-ear ossicles," *J. Acoust. Soc. Am. Suppl.* **1** **69**, S14.
- Funnell, W. R. J. (1983). "On the undamped natural frequencies and mode shapes of a finite-element model of the cat eardrum," *J. Acoust. Soc. Am.* **73**, 1657-1661.
- Funnell, W. R. J., Decraemer, W. F., and Khanna, S. M. (1987). "On the damped frequency response of a finite-element model of the cat eardrum," *J. Acoust. Soc. Am.* **81**, 1851-1859.
- Funnell, S. M., and Funnell, W. R. J. (1989). "An approach to finite-element modeling of the middle ear," *J. Acoust. Soc. Am. Suppl.* **1** **85**, S67.
- Gibbons, D. F. (1976). "Biomedical materials," in *CRC Handbook of Engineering in Medicine and Biology*, edited by D. G. Fleming and B. N. Feinberg (CRC, Cleveland), pp. 253-290.
- Guinan, J. J., Jr., and Peake, W. T. (1967). "Middle-ear characteristics of anesthetized cats," *J. Acoust. Soc. Am.* **41**, 1237-1261.
- Hayes, W. C. (1978). "Biomechanical measurements of bone," in *CRC Handbook of Engineering in Medicine and Biology, Section B, Instruments and Measurements, Vol. 1*, edited by B. N. Feinberg and D. G. Fleming (CRC, West Palm Beach), pp. 333-372.
- Khanna, S. M., and Tonndorf, J. (1972). "Tympanic membrane vibrations in cats studied by time-averaged holography," *J. Acoust. Soc. Am.* **51**, 1904-1920.
- Khanna, S. M., and Stinson, M. R. (1985). "Specification of the acoustical input to the ear at high frequencies," *J. Acoust. Soc. Am.* **77**, 577-589.
- Kirikae, I. (1960). *The Structure and Function of the Middle Ear* (University of Tokyo, Tokyo).
- Lang, S. B. (1969). "Elastic coefficients of animal bone," *Science* **165**, 287-288.
- McPherson, G. K., and Kriewall, T. J. (1980). "The elastic modulus of fetal cranial bone: a first step towards an understanding of the biomechanics of fetal head molding," *J. Biomech.* **13**, 9-16.
- Rabbitt, R. D., and Holmes, M. H. (1986). "A fibrous dynamic continuum model of the tympanic membrane," *J. Acoust. Soc. Am.* **80**, 1716-1728.
- Reilly, D. T., and Burstein, A. H. (1975). "The elastic and ultimate properties of compact bone tissue," *J. Biomech.* **8**, 393-405.
- Rice, J. C., Cowin, S. C., and Bowman, J. A. (1988). "On the dependence of the elasticity and strength of cancellous bone on apparent density," *J. Biomech.* **21**, 155-168.
- Roark, R. J., and Young, W. C. (1975). *Formulas for Stress and Strain, Fifth Edition* (McGraw-Hill, New York).
- Stinson, M. R. (1985). "The spatial distribution of sound pressure within scaled replicas of the human ear canal," *J. Acoust. Soc. Am.* **78**, 1596-1602.
- Yoon, H. S., and Katz, J. L. (1976). "Ultrasonic wave propagation in human cortical bone. II. Measurements of elastic properties and microhardness," *J. Biomech.* **9**, 459-464.